

Fugitive natural gas emissions in York, United Kingdom: Updating the parameters of existing algorithms to be based on instrumental limitations.

Thomas C. Moore¹, James R. Hopkins^{1,2}, Will S. Drysdale^{1,2}, Stuart Young¹, Sri Hapsari Budisulistiorini¹, Marvin D. Shaw^{1,2}, Mackenzie LeVernois³, James L. France^{3,4}, David Lowry³ and James D. Lee^{1,2}

¹Wolfson Atmospheric Chemistry Laboratories, University of York, York YO10 5DD, United Kingdom

²National Centre for Atmospheric Science, University of York, York YO10 5DD, United Kingdom

³Royal Holloway, University of London, Earth Sciences, Egham, United Kingdom

⁴Environmental Defence Fund Europe, Avenue des Arts 47-49, Brussels, Belgium

Correspondence to: james.lee@york.ac.uk

Abstract

Reducing methane emissions has become increasingly important in recent years due to its importance for radiative forcing. One area of particular interest is the oil and gas sector, which often results in fugitive emissions of methane from natural gas distribution. Previous studies have shown the ability to detect these emissions, by use of mobile surveys measuring methane. Some of these previous studies use ratios to secondary co-emitted compounds as a means of predicting the source of emission. This study aims to adapt existing algorithm parameters by investigating the limitations of equipment within the platform used for mobile surveys. These changes suggest that previous methods may underpredict the number of Leak Indications (LIs) by 53.5 % with the number of LIs detected with the old methodology being 27 and the new methodology detecting 58. The majority of these LIs were found to be emitting in a leak rate category of 0 - 2 L min⁻¹. Source appointment was included as a core step within the algorithm itself, this stage was shown to reduce the misassignment of LIs, suggesting the previous methodology may include emissions from pyrogenics and biogenics within their LI assignments.

1 Introduction

Following COP26 and the methane pledge (*European Commission and United States of America 2021*), methane and its emissions have received increased attention. The pledge states that the signatories will attempt to reduce their methane emissions by 30% of their 2020 levels by 2030. This was brought about due to increasing concern over the potency of methane as a greenhouse gas, with its warming potential 28 times greater than CO₂ over a 100-year timescale and 84 times

30 higher over a 20-year timescale (*IPCC, 2021*). 65 % of all methane emissions are thought to be anthropogenic in nature and
31 atmospheric methane has seen a consistent growth rate of > 5 ppb year⁻¹ since 2007, with 2021 and 2022 seeing growth rates
32 of 17.8 ppb year⁻¹ and 14 ppb year⁻¹ respectively (*Sauniois et al., 2025*), therefore understanding and mitigating
33 anthropogenic methane is a key goal to comply with the global methane pledge.

34
35 Of the anthropogenic emissions, the agricultural sector has the largest contribution towards atmospheric emissions (*Sauniois*
36 *et al., 2025*). Although there are means of reducing the emissions from these areas, including changing cattle, crop or land
37 management as well as changing the feedstock of the cattle, for example grass silage to maize silage (*Bačėninaitė et al.,*
38 *2022; Nisbet et al., 2025*), these changes may still require time to implement, so this sector cannot be the sole focus in order
39 to reach the 2030 deadline.

40
41 After agriculture, the largest contribution to anthropogenic emissions is from the energy sector with oil, natural gas and coal
42 having relatively similar contributions to methane emissions. Natural gas is of particular importance to the UK, with it being
43 the 19th largest country emitter of methane from the natural gas network (*Scarpelli et al., 2022*).

44
45 One of the sources of methane emissions from the natural gas network is fugitive emissions. A fugitive emission is an
46 unexpected or unwanted emission of gas from a pressurised network that is not detected by standard means (*Sotoodeh,*
47 *2021*). Within the natural gas network, they are commonly referred to colloquially as “Gas Leaks”, however the stigma
48 surrounding this term, both from industrial operators and the public, means the term fugitive emission is preferable to be
49 used where possible.

50
51 In the United Kingdom in 2023, 63.5 billion cubic metres of natural gas was consumed (*Energy Institute, 2024*). This is used
52 in a range of applications including; industrial use, electricity generation and domestic use. Of the UK’s natural gas
53 consumption, 33.8 % is from the domestic sector (*DESNZ, 2024*), with 73.8 % of households in England and Wales using
54 mains gas for either heating or cooking purposes (*Stewart et al., 2024*). In 2022, it was estimated that 117 kT of methane was
55 emitted as a result of fugitive emissions related to natural gas distribution (*NAEI, UK Emissions Data Selector*).

56 Within the UK, after natural gas is either produced or imported, it is first transported through the National Gas’ National
57 Transmission System (NTS), a network of over 5,000 miles of high-pressure steel pipes and more than 500 above ground
58 installations. This natural gas is then transported by one of several of the UK’s Gas Distribution Networks (GDNs), a GDN
59 first reduces the pressure from the NTS then oversees the pipework for pre-meter distribution of natural gas to homes and
60 businesses. The GDN responsible for York covers 2.7 million homes and businesses across the northeast of England and
61 northern Cumbria, which means the operation of tens of thousands of kilometres of pipework and therefore large unknowns
62 in the locations of fugitive emissions. To combat this, previous studies have implemented mobile measurement approaches
63 centred around the detection of areas with elevated methane.

64 1.1 Previous Mobile Measurement Methodology

65 There have been many previous studies that have attempted to design algorithms to detect fugitive emissions of natural gas,
66 all of which focus on locating enhancements in CH₄, the major component of natural gas. These algorithms define an
67 enhancement based on whether CH₄ mixing ratios are higher than a certain value (*Phillips et al., 2016*), are above a certain
68 percentile in measured readings (*Hopkins et al., 2016, Chamberlain et al., 2016*) or by using an outlier detection model
69 (*Keyes et al., 2020*).

70
71 The paper upon which our methodology is based, (*von Fischer et al., 2017*), defines Observed Peaks (OPs) as methane
72 enhancements > 110% of a 2.5-minute rolling background of the mean CH₄ concentrations two minutes before and after
73 each measured point, and that they occur over less than 160 m. Enhancements occurring within 5 seconds of each other are
74 grouped together. Mobile surveys are repeated multiple times and Leak Indications (LIs) are determined after grouping OPs
75 that occur within 20 m of one another and seeing which of these grouped clusters contain OPs from more than one mobile
76 survey. The LIs are then quantified into emission rates in L min⁻¹, using an equation derived from the results of a controlled
77 release experiment, shown in **Equation 1**.

$$78 \quad (\text{release rate} / L \text{ min}^{-1}) = 0.1178 + 0.08267 \times M - 0.005175 \times A + 0.08626 \times K \quad (\text{Eq. 1})$$

79 Where:

- 80 - M is the maximum CH₄ reading
- 81 - A is the peak area in ppm.metres
- 82 - K is the ratio of ppm.metres to maximum CH₄

83 This methodology was then further developed in (*Weller et al., 2019*). This changed the baseline such that it was the median
84 CH₄ value over 2.5 minutes, the spatial grouping of OPs to LIs changed from 20 m to 30 m and the quantification equation
85 changed to **Equation 2**.

$$86 \quad \ln(\text{excess CH}_4 / \text{ppm}) = -0.988 + 0.817 \times \ln(\text{emission rate} / L \text{ min}^{-1}) \quad (\text{Eq. 2})$$

87 Where the excess CH₄ term is the mean of all CH₄ enhancements associated with the resulting LI.

88 In (*Maazallahi et al., 2020*), it was proposed that the existing methodology categorised certain burning emissions as fugitive
89 emissions. To counter this an additional stage using CO₂ ratios with CH₄ was introduced to filter burning emissions.

90 Source attribution was also used in (*Fernandez et al., 2022*), using isotopic measurements of CH₄ in addition to ethane:
91 methane ratios.

92 Most recently in (*Tettenborn et al., 2025*), the approach was changed further, adapting the quantification equation to be
93 based on peak area as opposed to peak height. Resulting in the quantification equation shown in **Equation 3**.

$$94 \quad (\text{release rate} / L \text{ min}^{-1}) = \exp(1.292 \times \ln(\text{peak area}) - 2.377) \quad (\text{Eq. 3})$$

95 Where $\ln(\text{peak area})$ is the mean $\ln(\text{peak area})$ of all OPs within the LI cluster.

96 Variations of this algorithm have been used in many major cities across the US and Canada (*Ars et al., 2020; Weller et al.,*
97 *2022*) as well as European cities (*Defratyka et al., 2021; Fernandez et al., 2022; Wietzel et al., 2023; Vogel et al., 2024*) and

98 Asian cities (*Joo et al., 2024, Ueyama et al., 2025, Umezawa et al., 2025*). This paper attempts to detect smaller
99 enhancements of methane by adapting detection and clustering parameters to be specific to the limitations of the
100 instrumentation used. The paper also explores the effect of introducing a source attribution filter at the OP stage of the
101 algorithm and how this affects the number and the magnitude of LIs.

102 **2 Methodology**

103 **2.1 Instrumentation**

104 The WACL Air Sampling Platform (WASP) detailed in (*Wagner et al., 2021*) is the base for these measurements. The
105 sampling inlet for the WASP is located at the front of the van on the driver's side, meaning that the vehicle will sample the
106 centre of the road regardless of direction of travel. Since publication of (*Wagner et al., 2021*), the WASP has been updated to
107 include a Quark-Elec QK-AS07-0183 for GPS readings. For the measurements surrounding natural gas, the WASP was
108 equipped with a Los Gatos Microportable Greenhouse Gas Analyser (MGGA) for measurements of methane and CO₂,
109 Iterative Cavity Enhanced Differential Optical Absorption Spectrometer (ICAD) for measurements of NO_x (NO₂ + NO), and
110 an Aerodyne Tuneable Infrared Laser Direct Absorption Spectrometer (TILDAS) Laser Trace Gas Analyser for
111 measurements of ethane (*Yacovitch et al., 2014*). Measurements of ethane are calibrated using a three-point calibration of a
112 high standard of ethane (17.5 ppb), medium (2.5 ppb) and a zero, where calibration standard concentrations were confirmed
113 via GC-MS. For each mobile survey a calibration is performed before and after the mobile survey itself, a linear regression is
114 performed to find the slope and intercept of the calibration concentrations versus measured concentrations. The average is
115 taken for the two calibrations to account for instrument drift during the mobile survey and the resulting equation, **Equation**
116 **4**, is then used to apply a correction to ethane concentrations.

117

$$118 \quad C_2H_6_{corrected} = C_2H_6_{uncorrected} \cdot m + c \quad (\text{Eq. 4})$$

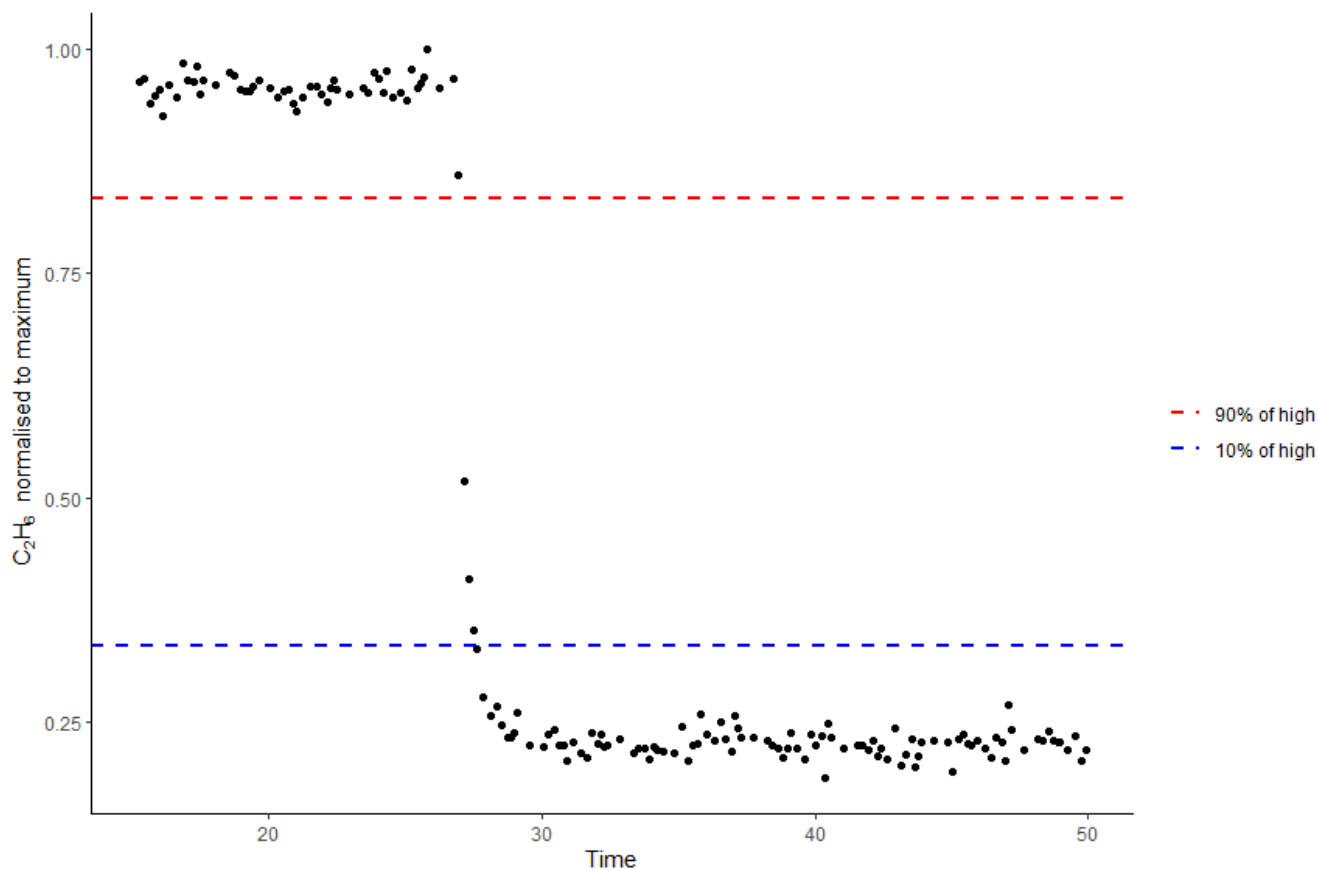
119 Where:

- 120 - m = Gradient of calibration concentration vs mean response averaged over the two calibrations
- 121 - c = Intercept of calibration concentration vs mean response averaged over the two calibrations

122 **2.1.1 Instrument Response Time**

123 Response time of the MGGA is reported as < 0.5 s from the manufacturer's specification. The response rate of the TILDAS
124 however was unknown. The TILDAS is capable of recording measurements at a rate of 10 Hz, however, the flow rate
125 through the instrument needed to be altered to make these measurements true to the 10 Hz values. Originally, the inlet to the
126 TILDAS had two valves in series, Stainless Steel Integral Bonnet Needle Valve, 0.37 Cv, 1/4 in. #SS-1RS4 and an electronic
127 Upstream Flow Control Valve, 10,000 sccm, 0.25 in. Tube, Viton Seal #0248A-10000SV which allows small changes to
128 maintain the internal pressure at 70 Torr. With the two valves in series, the instrument is unable to achieve a high enough

129 flow rate for true 10 Hz measurements. Moving the valves to be parallel, the instrument was able to achieve a flow rate close
130 to 5 Hz, at this point it was found that the pump was the limiting factor for the flow rate of the instrument.
131 These changes to increase the flow rate of the instrument were made to allow for a response time as close to that of the
132 MGGA as possible. To find the accurate response time of the TILDAS, an experiment was devised whereby a high
133 concentration of ethane (17.630 ± 0.715 ppb, measured via GC-MS) was flowed through the TILDAS and switched to
134 ambient air 10 times, on 2 separate valve setups, for a total of 20 repeats of low-high-low transitions in the concentration of
135 ethane. The transition times were located by eye and then the transition time to go from 90% of the maximum value to 10%
136 of the maximum value was calculated (*Symonds, 2017*), an example of the high to low transition with the 90 % and 10 %
137 limits is shown in **Figure 1**. The transition time on the first valve ranged from 0.7 – 1.1 s with a mean value of 0.9 s, the
138 second valve having responses ranging from 0.7 – 1.4 s also with a mean response of 0.9 s, giving confidence in a sub 1 s
139 response rate from the TILDAS and therefore showing the capability of a sub 1 s response in both instruments. The data
140 however was still averaged to 1 s with a 1 s clustering time due to the data now being limited by the data acquisition rate of
141 the WASP's GPS.



143

144

Figure 1: Example response transition of TILDAS high concentration to low concentration, normalised to maximum recorded response

145

146

2.1.2 Variation in methane measurements

147

Previous algorithms define an enhancement as being higher than 1.1 times a 2.5 minute rolling median background. This work however seeks to understand if this parameter holds true for the specific instrumentation used in the mobile surveys. To understand what this parameter may be, a variance experiment. The standard deviation of methane measurements over this period was calculated to understand the minimum detectable enhancement for the methane detection algorithm.

151

For 2 hours compressed air was flown through the Los Gatos MGGA, measured at a median value of 7.2 ppm, the standard deviation of these results was found to be 0.006 ppm. An enhancement criteria was proposed as 5 times this standard deviation divided by the median baseline, resulting in an enhancement criteria of 1.005 times the baseline. However, this assumes a stable baseline that is replicated in the field. In reality, when applying this enhancement criteria, it leads to the detection of enhancements that are too small to be reliably quantified. Instead, the methane mixing ratios measured during

155

156 each mobile survey, were collated and the standard deviation was calculated for each mobile survey. Again enhancement
157 criteria was calculated as anything larger than 5 times the standard deviation divided by the median of methane mixing
158 ratios, this was done for each mobile survey and resulted in a median enhancement criteria of 1.01 times the baseline.
159 However, as this would result in detection of enhancements that would be very small and could be diffuse or from
160 enhancements that occurred far from the roads and therefore harder to quantify as true natural gas emissions, a larger
161 enhancement criteria of 1.05 times the background was selected. This ensured there was still a large difference from the
162 original methodologies criteria, while still remaining within the instrumentation known variation.

163 **2.2 Driving Route**

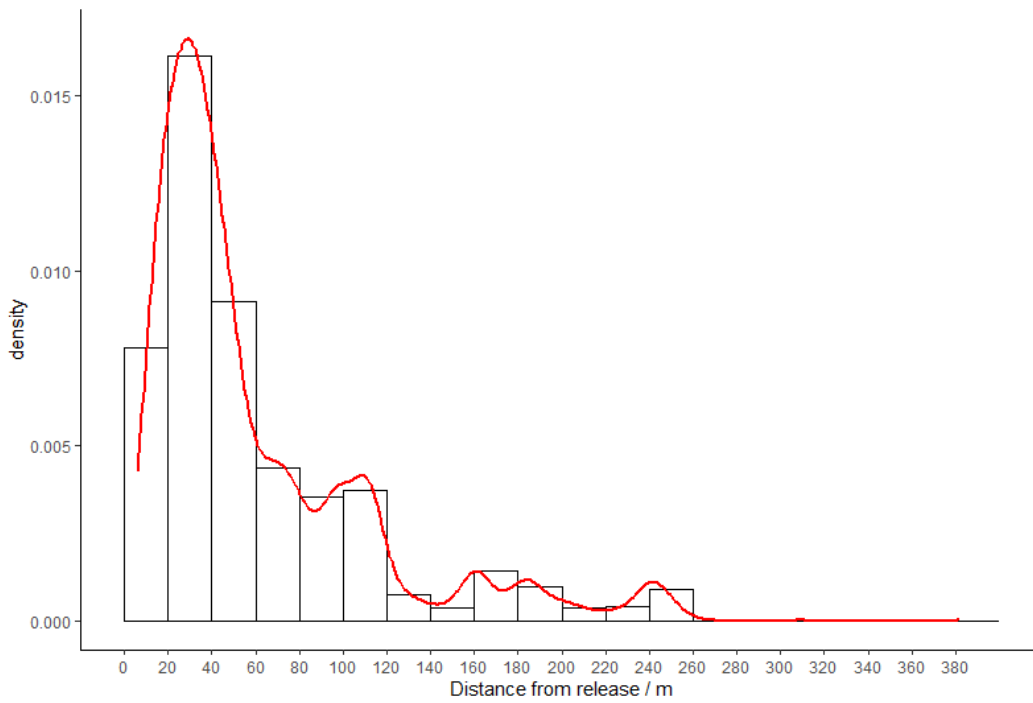
164 York is a city in the north-east of England with a population over 200,000. A driving campaign took place over two separate
165 weeks in May and June of 2024 resulting in 18 mobile surveys of a “flower petal” route, shown in *Figure 2*, staying within
166 the outer ring roads of the A64 and A1237 and mainly sampling residential areas of the city. The majority of the roads
167 sampled on the route were only driven in one direction but due to the position of the sampling inlet this allowed the middle
168 of the road to be sampled regardless of the direction of travel. The route was driven 18 times as, in order to capture > 90 %
169 of emissions, a route should be driven at least 5 - 8 times over separate days (*Luetschwager et al., 2021*). The route was
170 chosen as it covers multiple different neighbourhoods within York, but was not intended to be used to compare
171 measurements to the cities emissions inventory as it only covers a small fraction of the total miles of road within the York
172 urban area, 27 miles of a total 507 administered by the local authority (*Department for Transport, 2025*).

184 occurs only on OPs of the same source type, to further reduce the chance of comparing long standing thermogenic fugitive
185 emissions with possible nearby single occurrence pyrogenic or biogenic emissions.

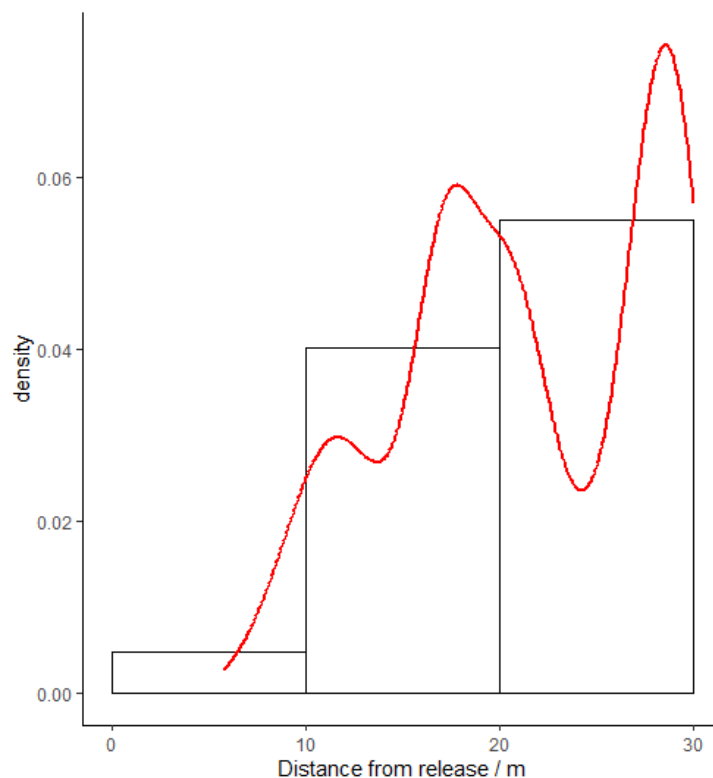
186 **2.4 Controlled Release Experiment**

187 To attain a quantification equation specific to the equipment used at York, a controlled release experiment was conducted at
188 the Bedford Aerodrome. The controlled release took place at the Bedford Aerodrome over 5 days in June of 2024. A
189 MiniCRF was deployed to manage releases of methane and ammonia, while a MidiCRF was deployed for releases of ethane.
190 In total, there were 41 releases lasting an average of 30 minutes each. Releases consisted of varying amounts of methane (0.2
191 - 70.48 L min⁻¹), ethane (0 - 7.01 L min⁻¹) and ammonia (0 - 7.87 L min⁻¹) to reflect a range of methane sources, including
192 natural gas and farm emissions. Releases were from a mixture of linear vertical releases, a multi emission point ring, multi
193 point source emissions and single point releases, occurring at heights ranging from ground level to 3 m elevation. Over the
194 course of the experiment wind speeds were measured using four Gill Met Pak Pro instruments deployed at 3 m, 6 m, 9 m and
195 12 m elevation, winds were recorded as 1 minute vector averages. Average wind speed over the 5 days was 3.87 m s⁻¹ with
196 wind speeds ranging from 0 - 9.75 m s⁻¹. During each release, an initial period was spent locating the plume before sampling
197 the plume at set distances for 10 repeats, the platform then stepped further away in distance for another set of 10 repeats, this
198 continued until the plume was either lost, or a lack of driveable ground was left available. It was noted that larger releases
199 were detectable further away, however, as the data from the controlled release was intended to be used in quantifying under-
200 road and near-road fugitive emissions of natural gas, a maximum distance of 30 m from the controlled release point was
201 applied, due to this reflecting the maximum road widths typically found within a city like York (*Essex Planning Officers*
202 *Association, 2018*).

203
204 Of the 41 releases conducted in the controlled release, only 26 releases were able to be used for processing data, this is due
205 to several reasons, including some releases not having detectable enhancements. Within these 26 releases, 3525 methane
206 enhancements were detected over distances between 5.8 m and 382.1 m from the release point; the majority of releases
207 detected further away from the release point were from higher emission rate releases. When this was filtered to include
208 enhancements up to a maximum of 30 m from the release point this resulted in 1226 enhancements from 23 mobile surveys.
209 Density plots of number of detected enhancements against distance from source are shown in *Figure 3* for all detected
210 enhancements and *Figure 4* for enhancements detected within 30 m from the source.



211
212 **Figure 3:** Density plot of number of detected enhancements against distance from release point
213



215

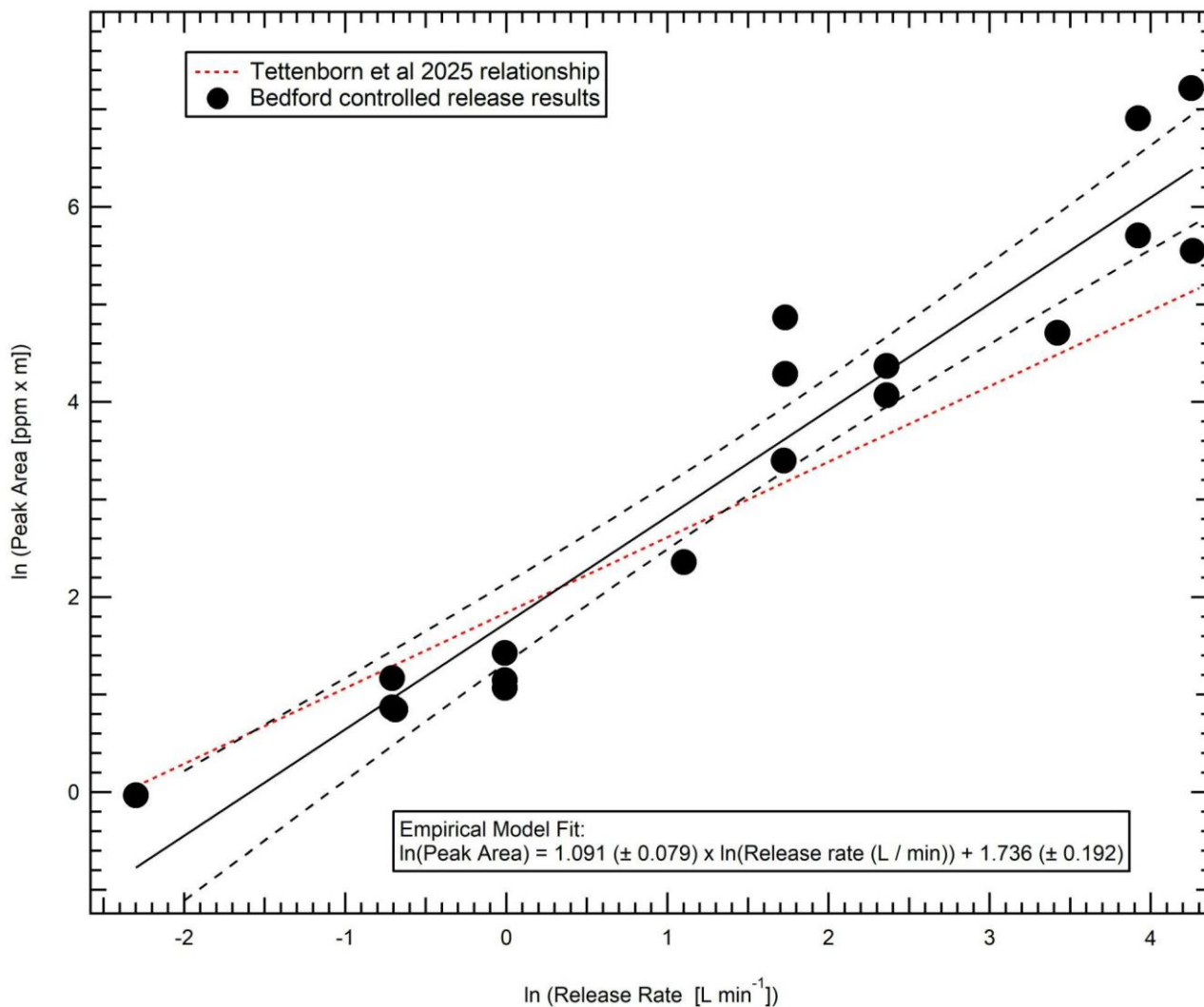
216 **Figure 4:** Density plot of number of detected enhancements against distance from release point (Limited to 0 – 30 m)217 **2.4.1 Quantification equation**

218 There has been much development and advancement in the last few years on the use and application of “Advanced Mobile
 219 Leak Detection” systems for natural gas emissions detection and reporting. The original methodologies, where algorithms
 220 were developed to convert peak height maxima of measured methane plumes to estimated emission rates (*Weller et al., 2019*)
 221 have been superseded with plume area algorithms (*Tettenborn et al. 2025*) which are instrument and vehicle speed agnostic.
 222 However, this is still not a precise conversion and can only be treated as a generalised guide to emissions estimation as factors
 223 such as wind, instrument inlet location and local variability due to buildings and unknown source locations.

224

225 In order to reduce the uncertainty for the WASP as much as possible, we present the results of a 1-week controlled release
 226 experiment conducted under variable wind conditions in a simple open field environment. Whilst this does not replicate the
 227 complex conditions of an urban setting, previous work in (*Tettenborn et al. 2025*) shows that combined results from both urban
 228 and open field settings can be combined to give a generalised trend to create their plume area emission algorithm. For the
 229 WASP, the setup is slightly different to the work in (*Tettenborn et al. 2025*), with the WASP’s inlet located on the driver’s

230 side at low elevation. This may influence the impact of vehicle turbulence on the measurements and the difference in elevation
 231 will lead to a different vertical section of the plume being sampled. A comparison between the results of the York controlled
 232 release, and the (Tettenborn *et al.* 2025) methodology averages are shown below in **Figure 5**. All data shown is for downwind
 233 transects where the plume was intercepted at a maximum of 30 m from the controlled release location. The plume area is
 234 calculated as a function of distance travelled (as opposed to time) to correct for vehicle speed differences as done in the original
 235 (Tettenborn *et al.* 2025) work.



236
 237 **Figure 5:** Peak area vs actual release rate for plume transects within 30m of release. Data shown is an average of multiple
 238 transects (at least 10) for each release.
 239

240 As it can be seen in **Figure 5**, whilst the general trend of increasing plume area with release rate is adhered to, the gradient of
241 the trend is steeper – implying that a near-ground based inlet is potentially more capable of ascribing differences in emission
242 rates.

243

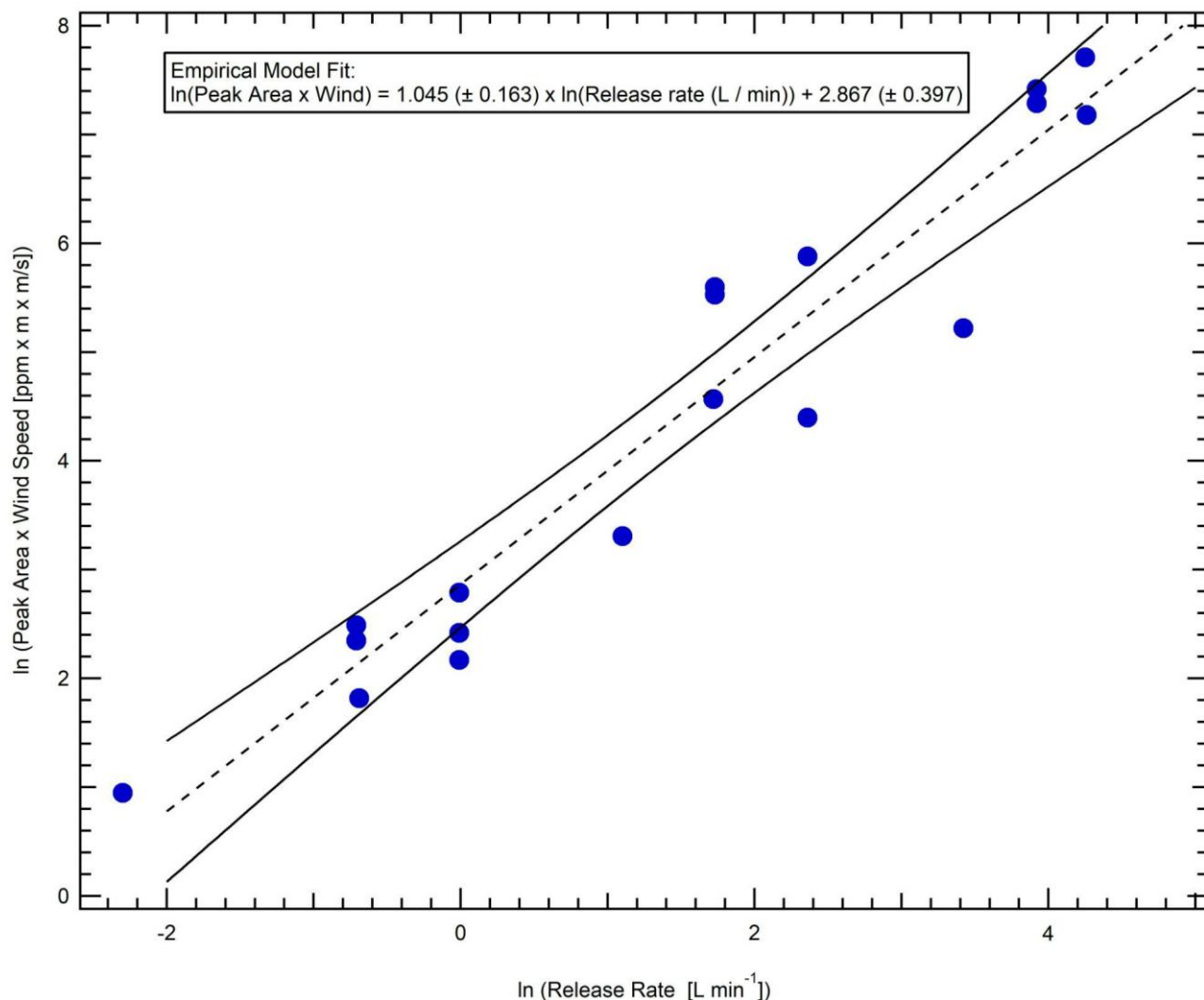
244 One of the expected limitations of these algorithmic methods is the assumption that the effect of windspeed is ignored, which
245 given the importance of windspeed in more distal emissions modelling such as Gaussian plume modelling from vehicles (*Dowd*
246 *et al. 2024*) may be an oversight. Using the 3 m mast, 1 Hz wind data (averaged to 1 minute data) located on site at the
247 controlled release, the wind data is incorporated into the algorithm to give a volumetric correlation with the release rate
248 according to **Equation 5**.

249

$$wind\ speed \times \int_{plume\ start}^{plume\ end} [CH_4] \quad (Eq. 5)$$

250 The results of the integration of the wind speed into the algorithm are shown below in **Figure 6**. Possibly somewhat
251 surprisingly, there is a slight decrease in the goodness of fit to the relationship – potentially due to plume dynamics close to
252 source not being immediately controlled by the atmospheric conditions, but the dynamics of the emission. This may also
253 provide evidence as to the reasons why the results of previous studies have ended up with metrics that would at first hand seem
254 unlikely to be able to produce reliable results from atmospheric dispersion principles. Given this result, that it seems to be as
255 robust to consider wind as to not, it may be prudent for future controlled release experiments to focus on recreating the
256 conditions of gas migration prior to emission to the atmosphere to see if this result still holds true.

257



259

260 **Figure 6:** Peak area x Wind speed vs actual release rate for plume transects within 30m of release. As with Figure 5, data
 261 shown is an average of multiple transects (at least 10) for each release.

262

263 Due to these findings, the quantification equation used within York mobile surveys is shown in **Equation 6**.

264

$$\ln(\text{release rate} / \text{L min}^{-1}) = 0.9167 \times \ln(\text{Peak Area}) - 1.7359 \quad (\text{Eq. 6})$$

265

266 Additionally, leak rates were then reported within bins, similar to that within (Tettenborn et al., 2025), where three
 267 possible bins were assigned; high (> 40 L min⁻¹), medium (6 - 40 L min⁻¹) and small (< 6 L min⁻¹). This was adapted
 268 for the York surveys, the small category was changed to 2 - 6 L min⁻¹ and a new category, very small, was introduced

269 which contained leak rates of 0 - 2 L min⁻¹. This change was introduced due to the lower enhancement criteria within
270 the York methodology which allows for detection of much smaller fugitive emissions.

271

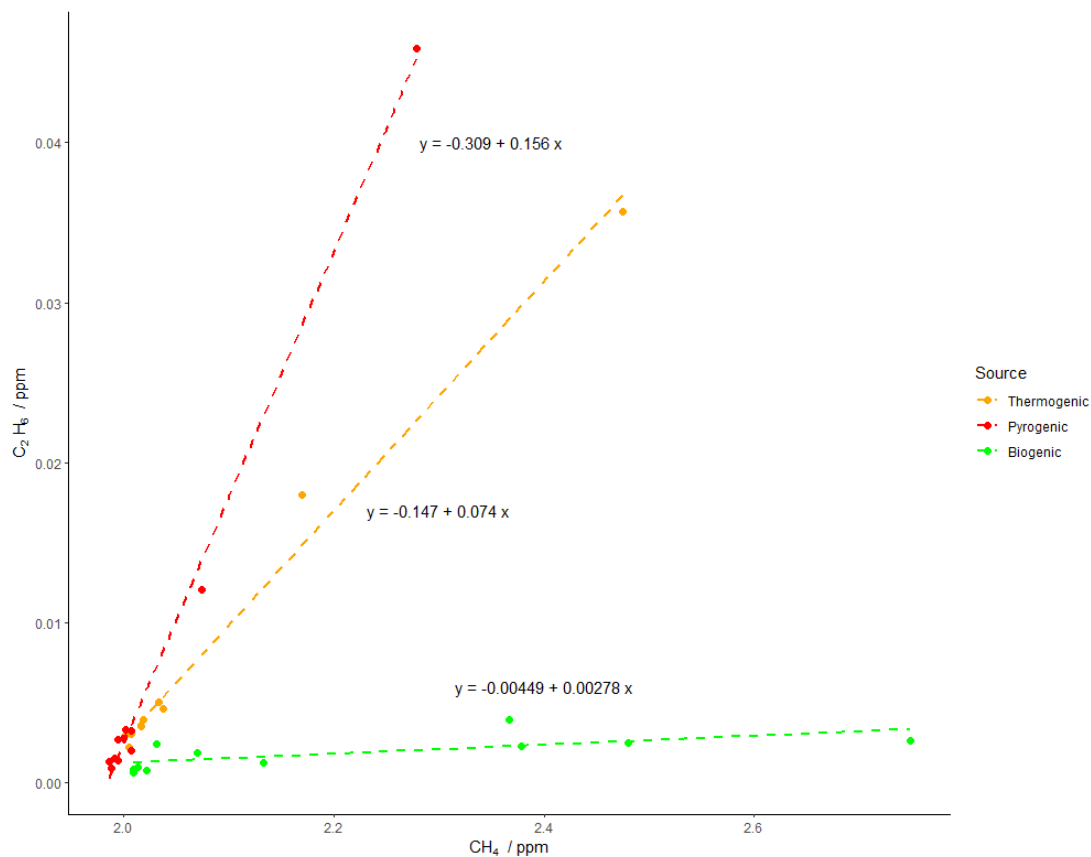
272 It is important to note that these results are only suitable for the specific set up utilised here and should not be more widely
273 applied without corroboration with other instruments or platform packages.

274 **2.4.2 Instrument Lag Time**

275 For each of the releases, the lag time between detecting an ethane enhancement and a methane enhancement was calculated.
276 Due to the response times of the instruments, it was expected that the TILDAS would respond to an enhancement before the
277 MGGA, however, this assumes that both instruments receive the same packet of air at the same time, while, in reality, the
278 packet of air will take a different amount of time to flow through manifold to each instrument. To find this more accurate lag
279 time of the instruments, the maximum methane enhancement for each pass was found, following this the maximum ethane
280 enhancement was found (that occurred within 5 seconds of the methane). The resulting 10 second window was selected as on
281 transects of the controlled release the van travelled at roughly 20 miles hour⁻¹. Over the course of 10 s (5 s either side of the
282 methane maximum) this would mean 85 m covered in the van, the average length of a transect being 180 m. The time lag
283 between ethane and methane showed that in most cases (88.1 %), maximum ethane concentration preceded maximum methane
284 concentration with a mean lag of 2.7 s before and a median of 3.8 s before. Observing a window of max methane to 5 s before
285 max methane resulted in a mean lag of 3.3 s from ethane to methane and a median lag of 3.9 s. This helped inform the detection
286 algorithm to look for maximum ethane within a window only up to 5s before the maximum methane. Density plots showing
287 the time lag of maximum ethane from maximum methane are shown in **Figure S2** for the full 10 second time window and
288 **Figure S3** for up to 5 seconds before the time of maximum measured methane.

289 **2.5 Source Appointment**

290 Source determination using ethane-methane ratios has been shown to be effective, due in part to the knowledge that ethane is
291 present in measurable quantities in thermogenic gas but not biogenic gas (*Fernandez et al., 2022*). ethane:methane (C₂:C₁)
292 ratios can be used in order to determine the source of a methane emission. Demonstrated in (*Yacovitch et al., 2014; Lowry et*
293 *al., 2020; Defratyka et al., 2021; Fernandez et al., 2022*), C₂:C₁ < 0.005 may be associated with biogenic sources, > 0.005 to
294 < 0.09 are thermogenic and > 0.1 are considered pyrogenic or combustion. Ideal examples of these relationships are shown
295 in **Figure 7**. In order to calculate these ratios methane and ethane values must first be aligned in time, due to them being
296 measured on separate instruments, the criterion for time alignment was discussed in **2.4.2**. Additionally, enhancements are
297 removed where the R² of CO₂:CH₄ is greater than 0.9 to ensure no combustion sources are wrongly assigned as thermogenic.



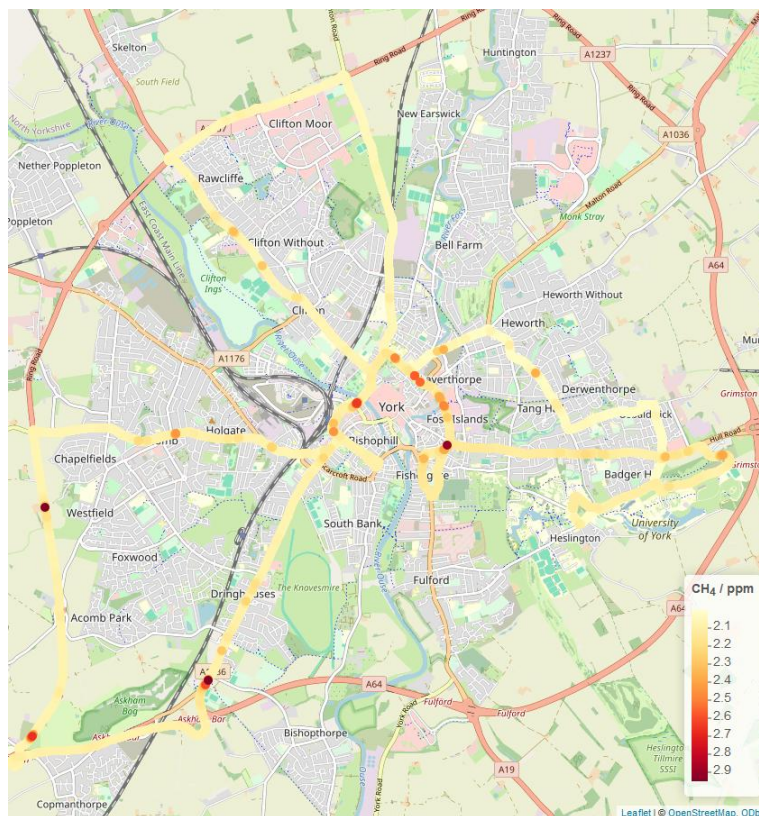
298
299 **Figure 7:** Relationship between CH_4 and C_2H_6 for three OPs of different source types located during the sampling
300 campaign.

301 **3 Results**

302 **3.1 Results of York mobile surveys**

303 17 mobile surveys were conducted across the route of York, the raw data was taken from 10 Hz files for methane (MGGA)
304 and ethane (TILDAS) and time averaged to 1 Hz data to be of the same response time as the WASPs other internal
305 components (e.g. GPS), a colour map of the resulting measured methane concentration is shown in **Figure 8**. The data was
306 then processed to remove data taken when speeds were 0 or > 40 miles hour⁻¹ as well as removing data within the area of
307 Wolfson Atmospheric Chemistry Laboratories due to this also being the location within which calibrations and other
308 instrument tests were conducted. A rolling 2.5-minute median background of CH_4 was then applied and enhancements were
309 determined as any CH_4 measurement taken that was greater than 1.05 times the calculated background. The enhanced
310 readings were then clustered such that any elevated reading within one second of another were assumed to correspond to the

311 same enhancement. These enhancements were then spatially averaged such that 468 OPs were detected over the course of
312 the 18 mobile surveys.
313



314
315 **Figure 8:** Colour map of CH₄ concentration from one of the York mobile surveys.
316

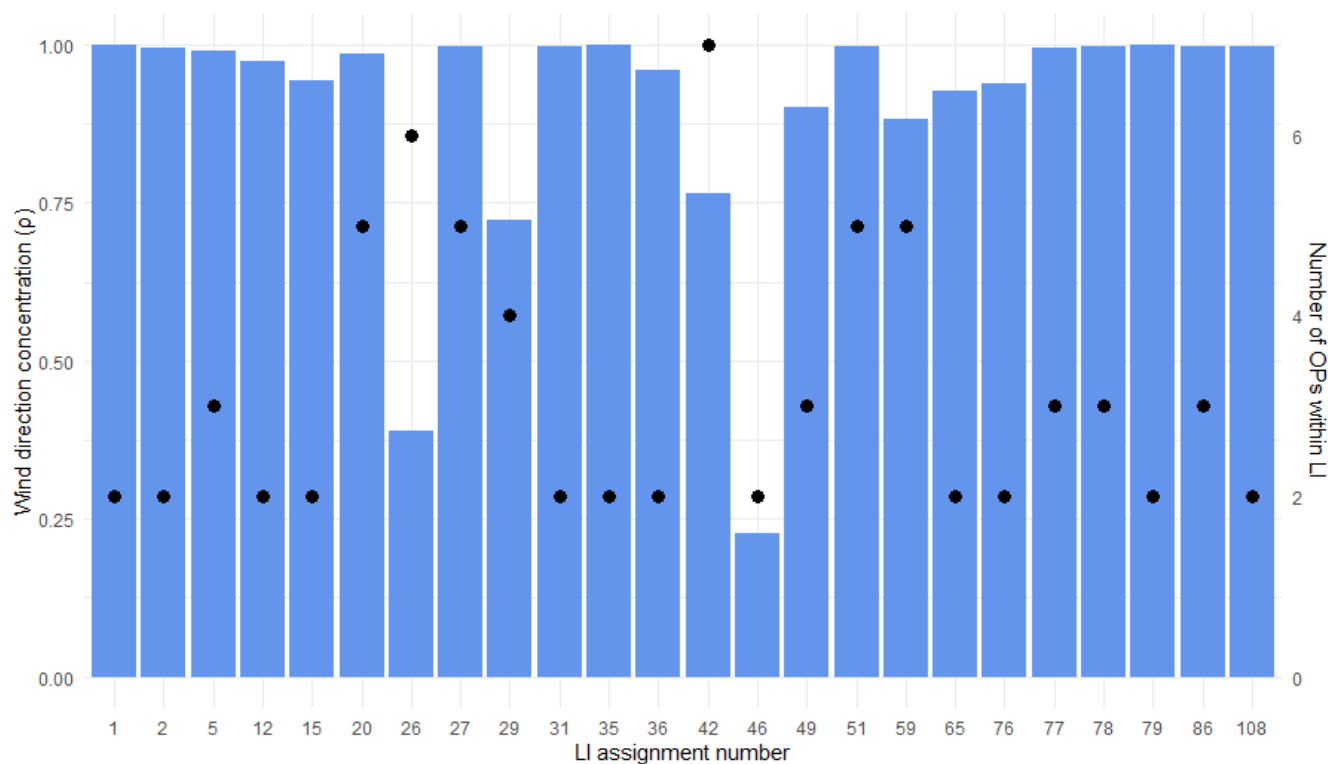
317 For each of these OPs the maximum ethane value was found from the time of maximum methane to 5 seconds prior. The two
318 instruments' data were then aligned for each OP such that time of maximum methane measurement was equal to time of
319 maximum ethane measurement. A linear regression was then taken of values from 5 seconds prior to the maximum methane
320 measurement to 5 seconds after and a source type was assigned such that $C_2:C_1 < 0.005$ is associated with biogenic sources, $>$
321 0.005 to < 0.09 are thermogenic and > 0.1 are considered pyrogenic or combustion.

322
323 This meant that of the 468 OPs, 177 (37.8 %) were found to be thermogenic in origin. Each Thermogenic OP was then clustered
324 to find others within 30 m of one another and filtered to ensure that clusters contained OPs occurring on at least two separate
325 mobile surveys, to remove any OPs occurring from an event happening on only one mobile survey. The remaining clusters
326 were then averaged into LIs such that the latitude and longitude were a weighted spatial average, resulting in 24 thermogenic
327 LIs from the 177 thermogenic OPs. Leak rate was determined using the equation present in 2.4.1 using the mean $\ln(\text{peak area})$

328 of all OPs within the LI cluster. The smallest leak rate was determined to be 0.01 L min⁻¹ and the largest being 4.13 L min⁻¹,
 329 when assigned to bins 2 were small (2 - 6 L min⁻¹) and 22 were very small (0 - 2 L min⁻¹). When the source type filter is
 330 omitted, this results in 58 LIs with leak rates ranging from 0.01 to 4.70 L min⁻¹, when assigned to bins 9 were small (2 - 6 L
 331 min⁻¹) and 49 were very small (0 - 2 L min⁻¹).

332 3.1.1 Industry applicability

333 As many gas distribution companies have signed up to voluntary emission reporting programmes, such as the Oil and Gas
 334 Methane Partnership (OGMP) 2.0, they are now obligated to report emissions through measurement-based methods. One of
 335 the most popular methods for such a reporting programme is through comprehensive, repeated vehicle-based measurement
 336 surveys of an operator's gas network. Here, we have a repeated route of measurements where thermogenic emissions have
 337 been reported at certain locations throughout the campaign. It is therefore interesting from a mitigation perspective to
 338 investigate how many times each of those thermogenic emissions were identified over the course of the campaign.



339 **Figure 9:** Wind direction consistency and number of OPs per Thermogenic leak indication
 340

341
 342 The effect of wind on detection of LIs was initially investigated by calculating the mean resultant length of wind directions
 343 when a Thermogenic OP was detected. This was calculated using *Equation 7*.

344

$$\rho = \frac{1}{n} \sqrt{\left(\sum_{i=1}^n \cos\theta_i\right)^2 + \left(\sum_{i=1}^n \sin\theta_i\right)^2} \quad (Eq. 7)$$

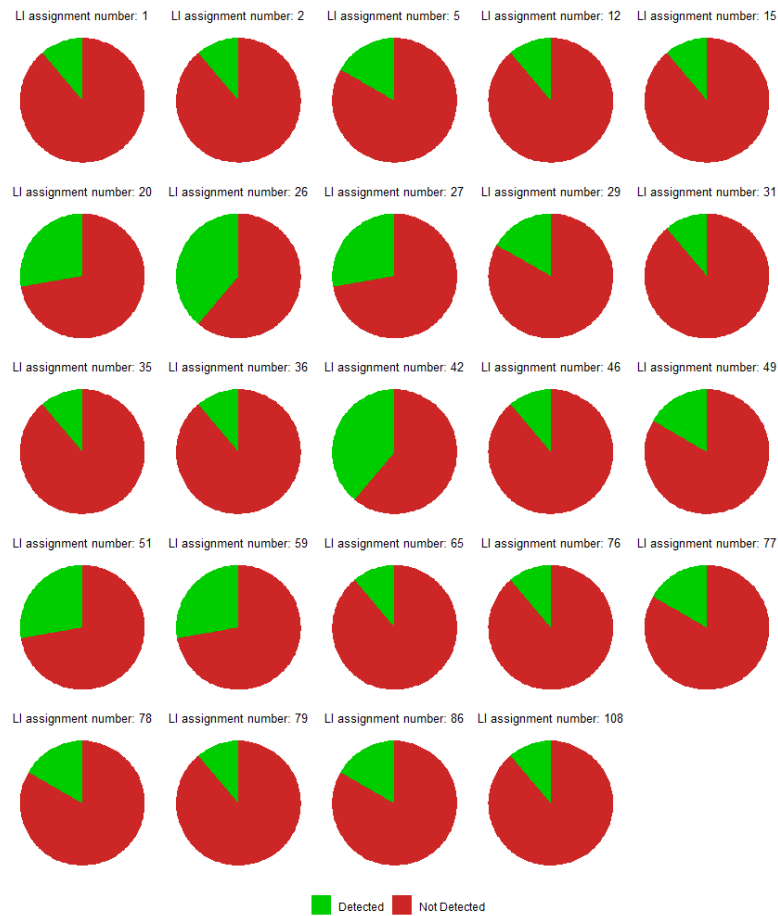
345

346 Where:

- 347 - ρ is mean resultant length
- 348 - n is number of data points
- 349 - θ_i is the angle in radians

350 For this analysis ρ is close to 1 when the wind directions are concentrated (similar) and close to 0 when more dispersed.

351 **Figure 9** shows that for the majority of LIs detected in York ρ is close to 1, suggesting that most LIs occur away from the
352 road and require correct wind direction in order to detect them.



353

354

355

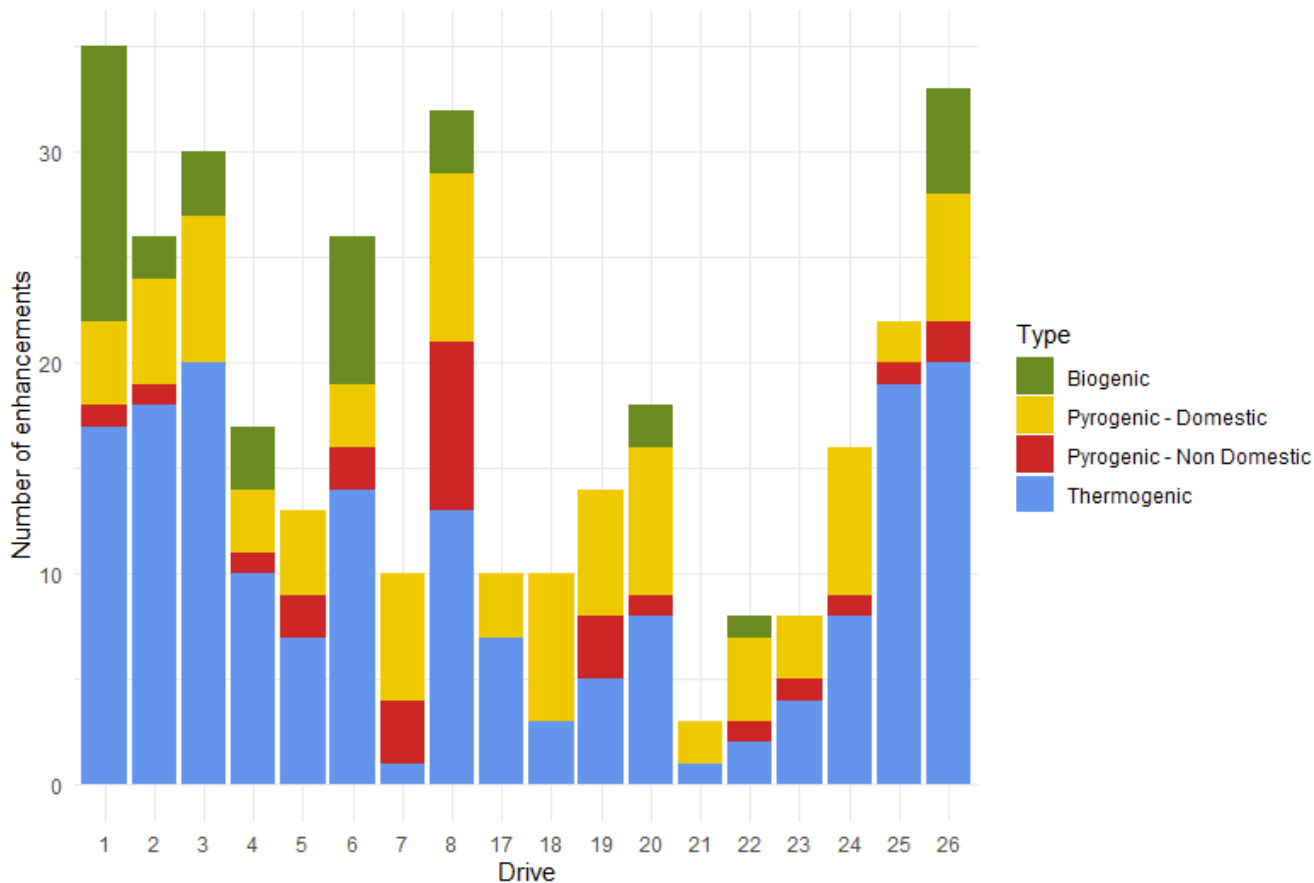
Figure 10: Pie charts of each LI showing number of mobile surveys they were detected vs not

356 The number of mobile surveys is a large factor in the probability of detecting an LI. Each LI requires the enhancement to be
357 detected on at least 2 separate mobile surveys, for the 24 LIs detected over the course of this campaign 12 LIs were detected
358 on 2 mobile surveys, 6 were detected on 3 mobile surveys, 4 on 5 mobile surveys and 2 on 7, this meant that the average
359 probability of detection was 0.18, detection versus non detection for each LI is demonstrated in **Figure 10**. This low
360 probability of detection highlights the need for surveys with multiple passes.

361 **3.2 Emissions from other sources**

362 While 177 of the 468 OPs were determined to be thermogenic, 39 were assigned as biogenic (8.3 %), 199 were pyrogenic
363 (41.8 %) and 53 were not able to be assigned a source type. NO_x:CO₂ ratios were investigated for the pyrogenic OPs using the
364 same methodology used for the CH₄:C₂H₆ source assignment. 115 of the 199 pyrogenic OPs were able to be analysed in this
365 way, 87 of these 115 OPs (75.7%) had a NO_x:CO₂ ratio < 0.88 x 10⁻³. This implied that the majority of pyrogenic emissions
366 did not originate from traffic but more likely emissions from domestic heat and power generation (such as emissions from
367 domestic boilers) (*Cliff et al., 2025*).

368 Emissions from pyrogenic and biogenic sources are compared to thermogenic source emissions at the OP stage on a mobile
369 survey by mobile survey basis due to the high unlikelihood of pyrogenics and biogenics being persistent emission sources, the
370 number of times each source type was detected per mobile survey is shown in **Figure 11**.



371 *Figure 11: Total number of enhancements from each source type for each of the mobile surveys.*

372
373
374 Thermogenics were the most frequently located source type on 13 of the 18 surveys, with mobile surveys 7, 18, 19, 21 and
375 22, finding pyrogenic emissions related to heating and cooking were the most frequently occurring source type.

376 3.3 Comparison to previous methods

377 The main alterations to this methodology from that present in (*Weller et al., 2019*) (and other studies that were based of this
378 method) were that enhancement criteria was changed from 1.1 times the baseline to 1.05 times the baseline, clustering by
379 time was changed such that emissions within 1 s of each other were clustered instead of those within 5 s. Finally, a source
380 determination stage was added as a core step in the algorithm as opposed to previous iterations that either had no source
381 determination stage or one that came later in the analysis. *Table 1* shows the effect that all of these changes to the
382 methodology make on the resulting detection of OPs and LIs.

Enhancement Criteria	Time Clustering Criteria / s	Source Determination Included?	Number of OPs	Number of LIs
110% of baseline	5	No	179	27
		Yes	66	6
	1	No	216	29
		Yes	79	7
105% of baseline	5	No	357	58
		Yes	144	23
	1	No	468	58
		Yes	177	24

Table 1: Number of detected OPs and LIs depending on changing algorithm parameters

384

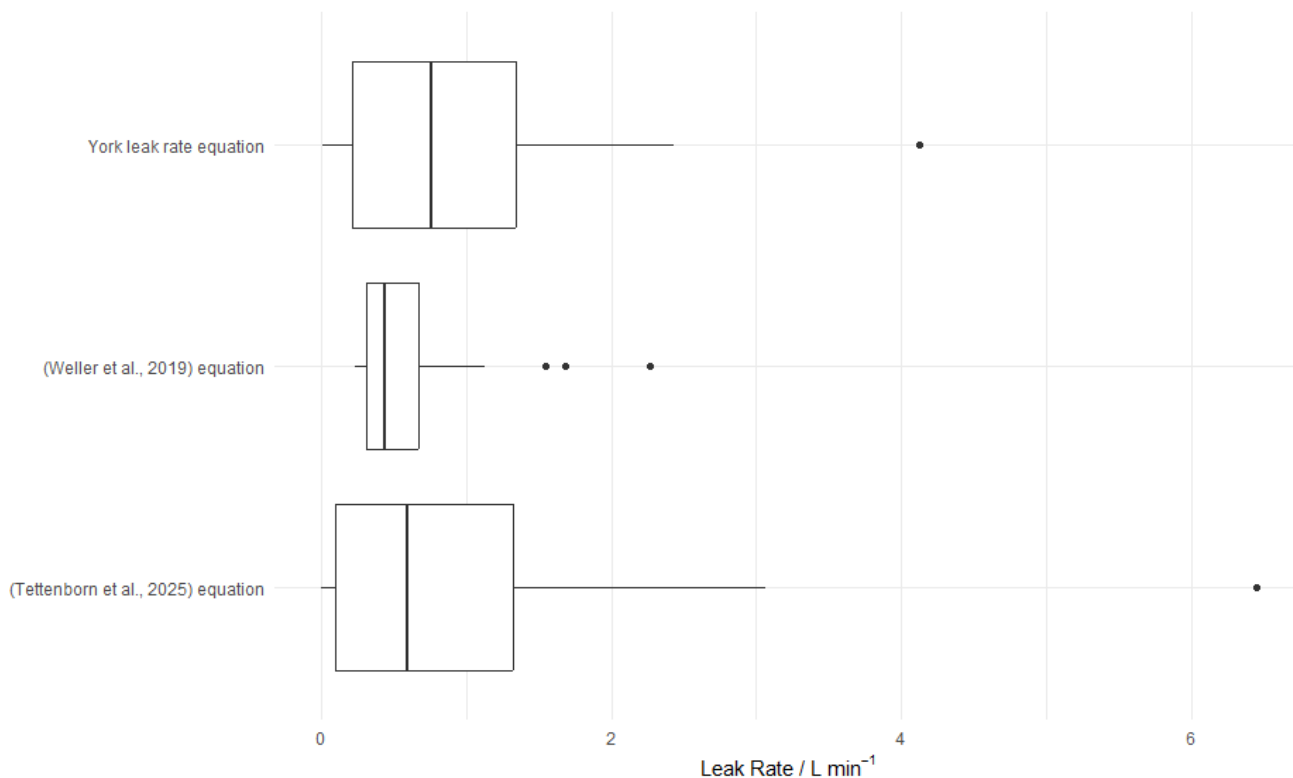
385

386 This shows the new methodology could locate more LIs. Binning into the leak rate categories of very small (0 - 2 L min⁻¹),
387 small (2 - 6 L min⁻¹), medium (6 - 40 L min⁻¹) and high (> 40 L min⁻¹) showed that of the 24 LIs in the new source filtered
388 methodology, 2 were small and 22 were very small. For the 58 LIs of the new non-filtered methodology, 9 were small and
389 49 were very small. For 27 LIs from the old non-filtered methodology 10 were small and 17 were very small. Finally, the 6
390 LIs from the old source filtered methodology, 1 was small and 5 were very small. This shows the old methodology requiring
391 an enhancement of 1.1 times the baseline with 5 s time clustering misses a large proportion of LIs that the newer
392 methodology, requiring an enhancement of 1.05 times the baseline with 1 s time clustering, detects. A large proportion of
393 these missed LIs occur in the very small category as expected with a smaller enhancement criteria. Source filtering shows
394 that regardless of criteria used less LIs will be detected with this method, this suggests previous methodologies that do not
395 use this stage may be mischaracterising some thermogenic enhancements as being permanent as they may instead be
396 detecting methane enhancements of differing source types that occur within the same vicinity of one another.

397 3.4 Comparison of alternate quantification approaches

398 As previously described, the quantification equation used within this body of work is based on the (Tettenborn *et al.*, 2025)
399 approach of using peak area to calculate the leak rate of a LI. However, previous works have used the quantification equation
400 present in (Weller *et al.*, 2019) which instead quantifies release rate based on peak height. This campaign's results were
401 reprocessed using each of these previous quantification equations in order to compare the effects of the updated parameters in
402 the York quantification equation to the original, present in (Tettenborn *et al.*, 2025) but also to explore the difference in
403 quantified leak rates from a peak height approach. As previously mentioned, the results of the York quantification approach

404 resulted in the 24 LIs being assigned to leak rate bins such that 2 were small and 22 were very small, the (Tettenborn et al.,
405 2025) equation results in 1 medium, 1 small and 22 very small and the (Weller et al., 2019) equation results in 1 small and 23
406 very small. The specific leak rates of LIs calculated with these three equations are presented in box-plots in **Figure 12**.



407
408 **Figure 12:** Comparison of calculated leak rates of LIs from each of the 3 quantification equations.
409

410 This shows that both the peak area approaches result in a much larger range of calculated leak rates from the LIs than from the
411 peak height approach present in (Weller et al., 2019). This suggests that the instrumentation used to detect CH₄ enhancements,
412 may result in low, wide peaks as opposed to higher, sharper peaks, thus explaining why leak rates are weighted much lower
413 from this method. The (Tettenborn et al., 2025) equation appears to be mostly consistent with the equation determined from
414 the York methodology, however there is slightly higher weighting of leak rates with the (Tettenborn et al., 2025) equation,
415 resulting in the 24 LIs changing from the assignments of 5 small and 19 to 1 medium, 5 small and 18 very small.

416 **4. Conclusions**

417 This study focused on using the limitations of surveying instrumentation to better inform a detection algorithm.
418 Enhancement criteria was determined by investigating the variance of the MGGA, although laboratory experiments
419 suggested the instrumentation was capable of detecting enhancements at a minimum of 1.005 times the baseline was

420 possible, in field experiments showed that enhancement criteria of 1.01 times the baseline was more likely the lower limit for
421 detection. However, for the surveys a criteria of 1.05 was selected so as to not incorporate small, diffuse emissions within the
422 analysis. Response rate of the instruments was calculated to inform the time window for clustering, with both MGGA and
423 TILDAS having sub one second response rate, the time clustering was instead limited to one second due to the limitations of
424 GPS data collection speed. These changes show previous methodologies would result in detection of 27 LIs compared to the
425 58 LIs using updated parameters (53.5 % less), the parameter change has also shown the ability to detect more LIs in all leak
426 rate categories, but in particular, the very small (0 - 2 L min⁻¹) category, where 17 of 27 LIs were located in the previous
427 methodology, but 46 of the 58 were located in the new methodology.

428 Source appointment proved to be a useful tool for predicting emissions directly related to natural gas, when source filtering
429 was introduced at the OP stage of detection, it resulted in only 41.4% of LIs still being detected as opposed to the non-source
430 filtered method.

431 Additionally source filtering has helped to highlight that although Thermogenic emissions from natural gas are the highest
432 contributor to methane emissions, pyrogenic emissions related to domestic heat and power generation also provide a high but
433 often overlooked contribution to a city's methane emissions.

434 The updating of the quantification equation from a peak height approach to a peak area approach results in a much wider
435 range of leak rates being calculated in the study, however these values are not as high as when quantified using the original
436 equation presented in (*Tettenborn et al., 2025*).

437 This new method has shown that with changing enhancement criteria and time clustering parameters, it is able to detect
438 many more LIs and that by applying a source type filter at the OP detection stage it is capable of reducing the incorrect
439 assignment of LIs. However, the methodology has ability to improve further, primarily by using instrumentation that is
440 capable of detecting methane and ethane on one instrument, so as to remove uncertainty related to time lag between the two
441 instruments, but secondly by having all instrumentation and hardware able to operate at a sub one second time rate in order
442 to reduce the time clustering parameter limit and further improve spatial resolution.

443 **Code / Data availability**

444 Code and data will be made available upon request.

445 **Author Contribution**

446 Contributed to conception: TM, JH, WD, JL. Contributed to data acquisition: TM, JH, WD, SY, SHB, MS, JL. Contributed to
447 analysis and interpretation of data: TM, JH, WD, SY, MLV, JF, JL. Initial draft of paper: TM. Subsequent drafts and/or
448 revisions to paper: TM, JH, WD, SY, DL, JF, JL. Approved the submitted version of this paper for publication: TM, JH, WD,
449 SY, SHB, MS, JF, DL, JL.

450 **Competing Interests**

451 The authors declare that they have no conflict of interest.

452 **Acknowledgements**

453 We would like to thank the INGENIOUS (Understanding the sourceS, traNsformations and fates of IndOor air pollUtantS)
454 project, NERC grant number NE/W002256/1, for providing access to their data in the early stages of the method development.
455 Additionally, we would like to thank both the National Physical Laboratory (NPL) and the MOMENTUM (Mobile
456 Observations and quantification of Methane Emissions to inform National Targeting, Upscaling and Mitigation) project, NERC
457 grant number NE/X014649/1, for organising and providing access to the controlled release experiment.

458 **References**

- 459 Ars, S., Vogel, F., Arrowsmith, C., Heerah, S., Knuckey, E., Lavoie, J., Lee, C., Pak, N.M., Phillips, J.L. and Wunch, D.,
460 Investigation of the spatial distribution of methane sources in the greater Toronto area using mobile gas monitoring systems.
461 Environ. Sci. Technol., 54(24), pp.15671-15679. <https://doi.org/10.1021/acs.est.0c05386>, 2020.
462
- 463 Bačėninaitė, D., Džermeikaitė, K. and Antanaitis, R., Global warming and dairy cattle: How to control and reduce methane
464 emission. Animals, 12(19), p.2687. <https://doi.org/10.3390/ani12192687>, 2022.
465
- 466 Chamberlain, S.D., Ingraffea, A.R. and Sparks, J.P., Sourcing methane and carbon dioxide emissions from a small city:
467 Influence of natural gas leakage and combustion. Environ. Pollut., 218, pp.102-110,
468 <https://doi.org/10.1016/j.envpol.2016.08.036>, 2016.
469
- 470 Cheng J, Schloerke B, Karambelkar B, Xie Y, Aden-Buie G. *leaflet: Create Interactive Web Maps with the JavaScript*
471 *'Leaflet' Library*. R package version 2.2.3.9000, <https://rstudio.github.io/leaflet/>, 2025
472
- 473 Cliff, S.J., Drysdale, W., Lewis, A.C., Møller, S.J., Helfter, C., Metzger, S., Liddard, R., Nemitz, E., Barlow, J.F. and Lee, J.
474 D., Evidence of Heating-Dominated Urban NO_x Emissions. Environ. Sci. Technol. 59(9), pp.4399-4408.
475 <https://doi.org/10.1021/acs.est.4c13276>, 2025
476
- 477 Defratyka, S.M., Paris, J.D., Yver-Kwok, C., Fernandez, J.M., Korben, P. and Bousquet, P., Mapping urban methane sources
478 in Paris, France. Environ. Sci. Technol., 55(13), pp.8583-8591. <https://doi.org/10.1021/acs.est.1c00859>, 2021
479

480 Department for Energy Security and Net Zero (DESNZ), Energy Trends: Natural Gas, Energy Trends September 2024,
481 https://assets.publishing.service.gov.uk/media/66f423473b919067bb48270e/Energy_Trends_September_2024.pdf (accessed
482 December 2024), 2024

483

484 Department for Transport: Road Length Statistics, RDL0102: Road length (miles) by road type and local authority in Great
485 Britain, <https://www.gov.uk/government/statistical-data-sets/road-length-statistics-rdl> (accessed April 2025), 2025
486

487 Dowd, E., Manning, A.J., Orth-Lashley, B., Girard, M., France, J., Fisher, R.E., Lowry, D., Lanoisellé, M., Pitt, J.R.,
488 Stanley, K.M., O’Doherty, S., Young, D., Thistlethwaite, G., Chipperfield, M.P., Gloor, E. and Wilson, C., First validation
489 of high-resolution satellite-derived methane emissions from an active gas leak in the UK. *Atmos. Meas. Tech.*, 17(5),
490 pp.1599–1615. <https://doi.org/10.5194/amt-17-1599-2024>, 2024.

491

492 Energy Institute, Statistical Review of World Energy, Natural gas consumption in the United Kingdom (UK) from 2003 to
493 2023 (in billion cubic meters),
494 https://www.energyinst.org/_data/assets/pdf_file/0004/1055542/EI_Stat_Review_PDF_single_3.pdf (accessed December
495 2024), 2023.

496

497 Essex Planning Officers Association, The Essex Design Guide, Design Details, 2018 Edition, V3,
498 <https://www.essexdesignguide.co.uk/media/2402/design-details-v3.pdf> (Accessed December 2024), 2018.
499

500 European Commission, United States of America, Global methane pledge,
501 <https://www.ccacoalition.org/sites/default/files/resources//Global%20Methane%20Pledge.pdf> (accessed July 2025), 2021
502

503 Fernandez, J.M., Maazallahi, H., France, J.L., Menoud, M., Corbu, M., Ardelean, M., Calcan, A., Townsend-Small, A., van
504 der Veen, C., Fisher, R.E. and Lowry, D., Street-level methane emissions of Bucharest, Romania and the dominance of
505 urban wastewater. *Atmos. Environ-X*, 13, p.100153. <https://doi.org/10.1016/j.aeaoa.2022.100153>, 2022.
506

507 Hopkins, F. M.; Kort, E. A.; Bush, S. E.; Ehleringer, J. R.; Lai, C. T.; Blake, D. R.; Randerson, J. T. Spatial patterns and
508 source attribution of urban methane in the Los Angeles Basin. *J. Geophys. Res.: Atmos.* 121 (5), 2490– 2507,
509 <https://doi.org/10.1002/2015JD024429>, 2016.

510

511 IPCC, 2021: Climate Change 2021: The Physical Science Basis. Contribution of Working Group I to the Sixth Assessment
512 Report of the Intergovernmental Panel on Climate Change[Masson-Delmotte, V., P. Zhai, A. Pirani, S.L. Connors, C. Péan,
513 S. Berger, N. Caud, Y. Chen, L. Goldfarb, M.I. Gomis, M. Huang, K. Leitzell, E. Lonnoy, J.B.R. Matthews, T.K. Maycock,

514 T. Waterfield, O. Yelekçi, R. Yu, and B. Zhou (eds.]. Cambridge University Press, Cambridge, United Kingdom and New
515 York, NY, USA, In press, <https://doi.org/10.1017/9781009157896>., 2021.

516

517 Joo, J., Jeong, S., Shin, J. and Chang, D.Y., Missing methane emissions from urban sewer networks. *Environ. Pollut.*, 342,
518 p.123101. <https://doi.org/10.1016/j.envpol.2023.123101>, 2024.

519

520 Keyes, T., Ridge, G., Klein, M., Phillips, N., Ackley, R. and Yang, Y., An enhanced procedure for urban mobile methane
521 leak detection. *Heliyon*, 6(10). <https://doi.org/10.1016/j.heliyon.2020.e04876>, 2020.

522

523 Lowry, D., Fisher, R. E., France, J. L., Coleman, M., Lanoisellé, M., Zazzeri, G., Nisbet, E. G., Shaw, J. T., Allen, G., Pitt,
524 J., and Ward, R. S.: Environmental baseline monitoring for shale gas development in the UK: Identification and geochemical
525 characterisation of local source emissions of methane to atmosphere, *Sci. Total Environ.*, 708, 134600,
526 <https://doi.org/10.1016/j.scitotenv.2019.134600>, 2020

527

528 Luetschwager, E., von Fischer, J.C. and Weller, Z.D., Characterizing detection probabilities of advanced mobile leak
529 surveys: Implications for sampling effort and leak size estimation in natural gas distribution systems. *Elem. Sci. Anth.*, 9(1),
530 p.00143. <https://doi.org/10.1525/elementa.2020.00143>, 2021.

531

532 Maazallahi, H., Fernandez, J.M., Menoud, M., Zavala-Araiza, D., Weller, Z.D., Schwietzke, S., Von Fischer, J.C., Denier
533 Van Der Gon, H. and Röckmann, T., Methane mapping, emission quantification, and attribution in two European cities:
534 Utrecht (NL) and Hamburg (DE). *Atmos. Chem. Phys.*, 20(23), pp.14717-14740. [https://doi.org/10.5194/acp-20-14717-](https://doi.org/10.5194/acp-20-14717-2020)
535 [2020](https://doi.org/10.5194/acp-20-14717-2020), 2020.

536

537 National Atmospheric Emissions Inventory (NAEI), UK Emissions Data Selector,
538 <https://naei.energysecurity.gov.uk/data/data-selector> . Selected emissions data for the year 2022, methane emissions related
539 to gas leakage from gas distribution 1B2b5. (accessed June 2025)

540

541 Nisbet, E.G., Manning, M.R., Lowry, D., Fisher R.E., Lan, X., Michel, S.E., France, J.L., Nisbet, R.E.R, Bakkaloglu, S.,
542 Leitner, S.M., Brooke, C., Röckmann, T., Allen, G., Denier van der Gon, H.A.C, Merbold, L., Scheutz, C., Woolley Maisch,
543 C., Nisbet-Jones, P.B.R., Alshalan, A., Fernandez, J.M. and Dlugokencky, E.J., Practical paths towards quantifying and
544 mitigating agricultural methane emissions, *Proceedings of the Royal Society A: Mathematical, Physical and Engineering*
545 *Sciences*, 481, 20240390, <https://doi.org/10.1098/rspa.2024.0390>, 2025

546

547 Phillips, N.G., Ackley, R., Crosson, E.R., Down, A., Hutyra, L.R., Brondfield, M., Karr, J.D., Zhao, K. and Jackson, R.B.,
548 Mapping urban pipeline leaks: Methane leaks across Boston. *Environ. Pollut.*, 173, pp.1-4.
549 <https://doi.org/10.1016/j.envpol.2012.11.003>, 2013.

550

551 Saunio, M., Martinez, A., Poulter, B., Zhang, Z., Raymond, P. A., Regnier, P., Canadell, J. G., Jackson, R. B., Patra, P. K.,
552 Bousquet, P., Ciais, P., Dlugokencky, E. J., Lan, X., Allen, G. H., Bastviken, D., Beerling, D. J., Belikov, D. A., Blake, D.
553 R., Castaldi, S., Crippa, M., Deemer, B. R., Dennison, F., Etiope, G., Gedney, N., Höglund-Isaksson, L., Holgersson, M. A.,
554 Hopcroft, P. O., Hugelius, G., Ito, A., Jain, A. K., Janardanan, R., Johnson, M. S., Kleinen, T., Krummel, P. B., Lauerwald,
555 R., Li, T., Liu, X., McDonald, K. C., Melton, J. R., Mühle, J., Müller, J., Murguía-Flores, F., Niwa, Y., Noce, S., Pan, S.,
556 Parker, R. J., Peng, C., Ramonet, M., Riley, W. J., Rocher-Ros, G., Rosentretter, J. A., Sasakawa, M., Segers, A., Smith, S. J.,
557 Stanley, E. H., Thanwerdas, J., Tian, H., Tsuruta, A., Tubiello, F. N., Weber, T. S., van der Werf, G. R., Worthy, D. E. J., Xi,
558 Y., Yoshida, Y., Zhang, W., Zheng, B., Zhu, Q. and Zhuang, Q., Global Methane Budget 2000 - 2020, *Earth Syst. Sci. Data*,
559 17, 1873-1958, <https://doi.org/10.5194/essd-17-1873-2025>, 2025.

560

561 Scarpelli, T.R., Jacob, D.J., Grossman, S., Lu, X., Qu, Z., Sulprizio, M.P., Zhang, Y., Reuland, F., Gordon, D. and Worden,
562 J.R., Updated Global Fuel Exploitation Inventory (GFEI) for methane emissions from the oil, gas, and coal sectors:
563 evaluation with inversions of atmospheric methane observations. *Atmos. Chem. Phys.*, 22(5), pp.3235-3249.
564 <https://doi.org/10.5194/acp-22-3235-2022>, 2022.

565

566 Sotoodeh, K., Why packing adjustment cannot stop leakage: Case study of a ball valve failing to seal after packing
567 adjustment during fugitive emission as per ISO 15848-1. *Eng. Fail. Anal.*, 130, p.105751.
568 <https://doi.org/10.1016/j.engfailanal.2021.105751>, 2021.

569

570 Stewart I., Bolton P.; Households off the gas-grid and prices for alternative fuels; House of Commons Library,
571 <https://researchbriefings.files.parliament.uk/documents/CBP-9838/CBP-9838.pdf> (accessed December 2024), 2024.

572

573 Symonds, J, August 15 2017, On Instrument Time Response: What it means, what it isn't, and why it matters, [Article],
574 LinkedIn. <https://www.linkedin.com/pulse/instrument-time-response-what-means-why-matters-jonathan-symonds/>
575 (Accessed November 2024)

576

577 Tettenborn J., Zavala-Araiza D., Stroeken, D., Maazallahi, H., van der Veen, C., Hensen, A., Velzeboer, I., van den Bulk, P.,
578 Gillespie, L., Ars, S., France, J., Lowry, D., Fisher, R. and Röckmann, T., Improving consistency in methane emission
579 quantification from the natural gas distribution systems across measurement devices. *Atmos. Meas. Tech.*, 18, 3569–3584,
580 <https://doi.org/10.5194/amt-18-3569-2025>, 2025

581 Ueyama, M., Umezawa, T., Terao, Y., Lunt, M. and France, J.L., Evaluating urban methane emissions and their attributes in
582 a megacity, Osaka, Japan, via mobile and eddy covariance measurements. *Atmos. Chem. Phys.*, 25(19), pp.12513–12534.
583 <https://doi.org/10.5194/acp-25-12513-2025>, 2025.

584 Umezawa, T., Terao, Y., Ueyama, M., Kameyama, S., Lunt, M. and France, J.L., Measurement report: Mobile measurements
585 to estimate urban methane emissions in Tokyo. *Atmos. Chem. Phys.*, 25(23), pp.18015–18029. [https://doi.org/10.5194/acp-](https://doi.org/10.5194/acp-25-18015-2025)
586 [25-18015-2025](https://doi.org/10.5194/acp-25-18015-2025), 2025.

587 Vogel, F., Ars, S., Wunch, D., Lavoie, J., Gillespie, L., Maazallahi, H., Röckmann, T., Necki, J., Bartyzel, J., Jagoda, P. and
588 Lowry, D., Ground-Based Mobile Measurements to Track Urban Methane Emissions from Natural Gas in 12 Cities across
589 Eight Countries. *Environ. Sci. Technol.*, 58(5), pp.2271–2281. <https://doi.org/10.1021/acs.est.3c03160>, 2024.

590

591 von Fischer, J.C., Cooley, D., Chamberlain, S., Gaylord, A., Griebenow, C.J., Hamburg, S.P., Salo, J., Schumacher, R.,
592 Theobald, D. and Ham, J., Rapid, vehicle-based identification of location and magnitude of urban natural gas pipeline
593 leaks. *Environ. Sci. Technol.*, 51(7), pp.4091–4099. <https://doi.org/10.1021/acs.est.6b06095>, 2017.

594

595 Wagner, R. L., Farren, N. J., Davison, J., Young, S., Hopkins, J. R., Lewis, A. C., Carslaw, D. C., and Shaw, M. D.:
596 Application of a mobile laboratory using a selected-ion flow-tube mass spectrometer (SIFT-MS) for characterisation of
597 volatile organic compounds and atmospheric trace gases, *Atmos. Meas. Tech.*, 14, 6083–6100, [https://doi.org/10.5194/amt-](https://doi.org/10.5194/amt-14-6083-2021)
598 [14-6083-2021](https://doi.org/10.5194/amt-14-6083-2021), <https://doi.org/10.5194/amt-14-6083-2021>, 2021.

599

600 Weller, Z.D., Yang, D.K. and von Fischer, J.C., An open source algorithm to detect natural gas leaks from mobile methane
601 survey data. *PLoS One*, 14(2), p.e0212287. <https://doi.org/10.1371/journal.pone.0212287>, 2019.

602

603 Weller, Z.D., Im, S., Palacios, V., Stuchiner, E. and von Fischer, J.C., Environmental injustices of leaks from urban natural
604 gas distribution systems: patterns among and within 13 US metro areas *Environ. Sci. Technol.*, 56(12), pp.8599–8609.
605 <https://doi.org/10.1021/acs.est.2c00097>, 2022.

606

607 Wietzel, J.B. and Schmidt, M., Methane emission mapping and quantification in two medium-sized cities in Germany:
608 Heidelberg and Schwetzingen. *Atmos. Environ-X*, 20, p.100228. <https://doi.org/10.1016/j.aeaoa.2023.100228>, 2023.

609

610 Yacovitch, T.I., Herndon, S.C., Roscioli, J.R., Floerchinger, C., McGovern, R.M., Agnese, M., Pétron, G., Kofler, J.,
611 Sweeney, C., Karion, A. and Conley, S.A., Demonstration of an ethane spectrometer for methane source
612 identification. *Environ. Sci. Technol.*, 48(14), pp.8028–8034. <https://doi.org/10.1021/es501475q>, 2014.